Original paper

Investigation of biochemical composition of adrenal gland tumors by means of FTIR

Joanna Dudala[1], Magdalena B. Białas[2], Magdalena Szczerbowska-Boruchowska[1], Monika Bereza-Buziak[3], Andrzej Budzynski[4], Alicja Hubalewska-Dydejczyk[3], Maciej Kolodziej[5], Michal Pedziwiatr[4], Marek Lankosz[1]

[1]Faculty of Physics and Applied Computer Science, AGH University of Science and Technology, Krakow, Poland
[2]Chair of Pathomorphology, Jagiellonian University, Medical College, Krakow, Poland
[3]Department of Endocrinology, Jagiellonian University, Medical College, Krakow, Poland
[4]2nd Department of General Surgery, Jagiellonian University, Medical College, Krakow, Poland
[5]University Hospital, Krakow, Poland

The application of Fourier transform infrared (FTIR) microspectroscopy for the analysis of biomolecular composition of adrenal gland tumors is described. Samples were taken intraoperatively from three types of adrenal lesions: adrenal adenoma (ACA), adrenal cortical hyperplasia (ACH), both derived from adrenal cortical cells, and pheochromocytoma (Ph) derived from chromaffin cells of the adrenal medulla. The specimens were cryo-sectioned and freeze-dried. Since the investigated lesions originated from different cell types, it was predictable that they might differ in biomolecular composition. The experimental results were used to determine which absorption bands differentiate the analyzed samples the most. The main difference was observed in the lipid functional groups. The experimental results indicated that the level of lipids was higher in both the adenoma and the hyperplasia samples compared to pheochromocytomas. In contrast, the level of proteins was higher in the pheochromocytomas. Furthermore, differences within the range of nucleic acids and carbohydrates were observed in the studied adrenal gland tumor types.

Key words: adenoma, adrenal gland, FTIR, hyperplasia, pheochromocytoma, tumor.

Introduction

Adrenal gland

The adrenal glands (suprarenal glands) are paired, small endocrine organs located in the retroperitoneum on the kidney surface. They consist of the cortex and medulla, which differ in their development and function. The adrenal cortex mainly plays a role in the regulation of water and electrolyte balance (via production of mineralocorticoids) and modulates metabolism of proteins, carbohydrates and fat (via production of glucocorticoids), while the adrenal medulla is involved in reacting to stress and enabling rapid adaptation to changes in the environment. The adrenal medulla is composed of chromaffin cells which synthesize and secrete catecholamines (mainly epinephrine). Pathological lesions developing in adrenal glands differ in their nature depending on whether they are derived from cortical or medullar tissue. The most common cortical conditions include different types of adrenal cortical hyperplasia (ACH), a non-neoplastic lesion characterized by an increase in the number of cortical cells, usually forming one or

many nodules (tumors) and causing an increase in size of the adrenal gland, as well as adrenal cortical adenoma (ACA) and adrenal cortical carcinoma (ACC), which are neoplastic lesions, benign and malignant respectively. The most common pathological condition associated with adrenal medulla is pheochromocytoma (Ph, adrenal gland paraganglioma) [1].

The aim of this study was to compare the differences between cortical and medullar tumors using Fourier transform infrared (FTIR) as a method enabling characterization of biomolecular composition in tissues. We also tried to find any biochemical differences between non-neoplastic and neoplastic cortical adrenal lesions.

Fourier transform infrared as a potential supporting method for the diagnosis of adrenal gland diseases

Due to various processes leading to tumor progression, the affected tissue can be modified anatomically and biochemically. The growing tumor mass needs more oxygen and glucose compared to the healthy tissue. This results in new capillary vessel formation (angiogenesis) and changes of biochemical composition of tumor tissue compared to corresponding non-neoplastic tissue [2, 3, 4]. Histopathological examination of a biopsy sample or intraoperative material is a routinely used method of making a diagnosis. It is directed at the anatomical structure, architectural features and cytological changes of studied tissue. Nevertheless, the literature review revealed that FTIR microspectroscopy is used as a complementary method of pathological state diagnosis [5, 6, 7, 8, 9, 10]. The idea of FTIR application for medical surveillance is to find out the specific biomolecular markers which can differentiate non-neoplastic and pathological (neoplastic) tissues.

Fourier transform infrared measurements and interpretations

Infrared spectroscopy is based on the physical phenomenon of resonant absorption of infrared light through vibrating molecules. Cellular biomolecules such as carbohydrates, lipids, proteins and nucleic acids absorb within the range of mid-IR (from about 400 cm^{-1} to 4000 cm^{-1} [11]). The individual absorption bands are related to several characteristic bonds of biomolecules. Tentative assignments of the frequencies of bands present in IR spectra measured for tissue samples are shown in Table I.

The problem is that the absorption bands from different molecules can overlap; hence it is very difficult to analyze unequivocally the sample biocomposition. Nevertheless, using FTIR spectroscopy as a diagnostic tool is aimed at discovering the differences between healthy and abnormal tissue. Comparing spectra derived from several tissue specimens, it is possible to find the absorption bands which differentiate samples the most. Consequently the biochemical processes causing that difference may be revealed.

Table I. Tentative assignments of the band frequencies present in IR absorption spectra [15, 16]

Frequency (cm^{-1})	Assignments
~3500-3200	ν(O–H): (hydroxyl groups)
~3200-3300	ν(N–H): (proteins, amide A)
~3080	ν(N–H): (proteins, amide B)
~3020-3000	ν(=CH): (olefinic) unsaturated fatty acids, cholesterol esters
~2990-2950	$\nu_{as}(CH_3)$: (methyl) phospholipids, cholesterol esters, fatty acids
~2950-2880	$\nu_{as}(CH_2)$: (methylene) phospholipids, long chain fatty acids
~2880-2860	$\nu_{s}(CH_3)$: (methyl) phospholipids, fatty acids
~2870-2830	$\nu_{s}(CH_2)$: (methylene) phospholipids, long chain fatty acids
~1739-1713	ν(C=O): phospholipids, cholesterol esters, glycerides
~1713-1589	ν(C=O): proteins, lipids
~1654	amide I
~1589-1474	δ(N–H): proteins, lipids
~1545	amide II
~1480-1430	$\delta_{as}(CH_3)$, $\delta_{as}(CH_2)$, $\delta_{s}(CH_3)$, $\delta_{s}(CH_2)$: phospholipids, fatty acids, glycerides
~1420-1370	ν(COO^-): (carboxylate ions) amino-acids
~1280-1220	ν(P=O): (phosphate) phospholipids
~1300-900	ν(C–O): saccharides, glucose, lactate

ν – *stretching vibrations (s – symmetric, as – asymmetric);* δ – *bending (scissoring) vibrations*

Material and methods

Sample preparation

In our study the archival tissue samples from different types of adrenal gland lesions were used. They were obtained from the Pathomorphology Department, Medical College, Jagiellonian University in Krakow, Poland. The study was approved by the Jagiellonian University Bioethical Committee (KBET/82/B/2010). The specimens were taken intraoperatively from patients with adenoma and hyperplasia – both derived from the cortical part of the adrenal gland – and pheochromocytoma derived from the adrenal medulla. The specimens were cut into sections 10 μm thick in a cryo-microtome, mounted on silver-coated sample supports (Low-e MirrIR, Kevley Technologies) and freeze-dried at –80°C. It has been demonstrated that dried tissue mounted onto this sample support is durable, and the applied method is used as routine procedure of tissue sample preparation for infrared microspectroscopy [12].

IR data collection and spectra analysis

The measurements were carried out at the Faculty of Physics and Applied Computer Science at the AGH University of Science and Technology in Krakow. The measurements were performed using the IR microscope (Nicolet Continuum – Thermo Scientific) coupled with an FTIR spectrometer (Nicolet 8700 – Thermo Scientific). The scientific instrumentation was equipped with a ceramic infrared radiation source (the range of 20-9600 cm^{-1}) and an MCT detector (mercury cadmium telluride, $HgCdTeO_2$), liquid nitrogen cooled. The samples were analyzed in reflection mode with a beam defined by the aperture 20 μm × 20 μm and spatial resolution steps of 15 μm. The spectra were collected for the wavenumber range from 800 cm^1 to 4000 cm^{-1} with a spectral resolution of 8 cm^{-1} and 150 scans collected per spectrum.

The data collection was performed with the OMNIC software (v.8.0), which was also applied, apart from the CytoSpec (v.1.2) software, for spectral analysis. For quantitative analysis OPUS (v.6.5) was used. For the statistical analysis the STATISTICA (v.10) software was used, while for the spectra presentation the ORIGIN (v.9.0) software was applied.

To select spectra of good quality for further semi-quantitative analysis the criterion described by Lash [13] was applied. Taking into account the reflection mode of infrared measurement, the total absorption for the 10 μm thick biological samples in the spectral range from 950 to 1750 cm^{-1} should vary from 125 to 625 arbitary units.

The CytoSpec software was used to check the thickness criterion. An exemplary result of application of this criterion for measured tissue area is shown in Fig. 1. Black pixels mean the points which do not fulfill the thickness criterion, and consequently they have not been taken into account for further analysis. From the homogeneous part of the specimen 20 representative points (fulfilling the sample thickness criterion) were selected for the analysis. Moreover, visible scattering manifestations in the IR absorption spectra, as presented in Fig. 2, were avoided. It is due to the fact that distortion of the baseline ("sinusoidal baseline") can affect the semi-quantitative results.

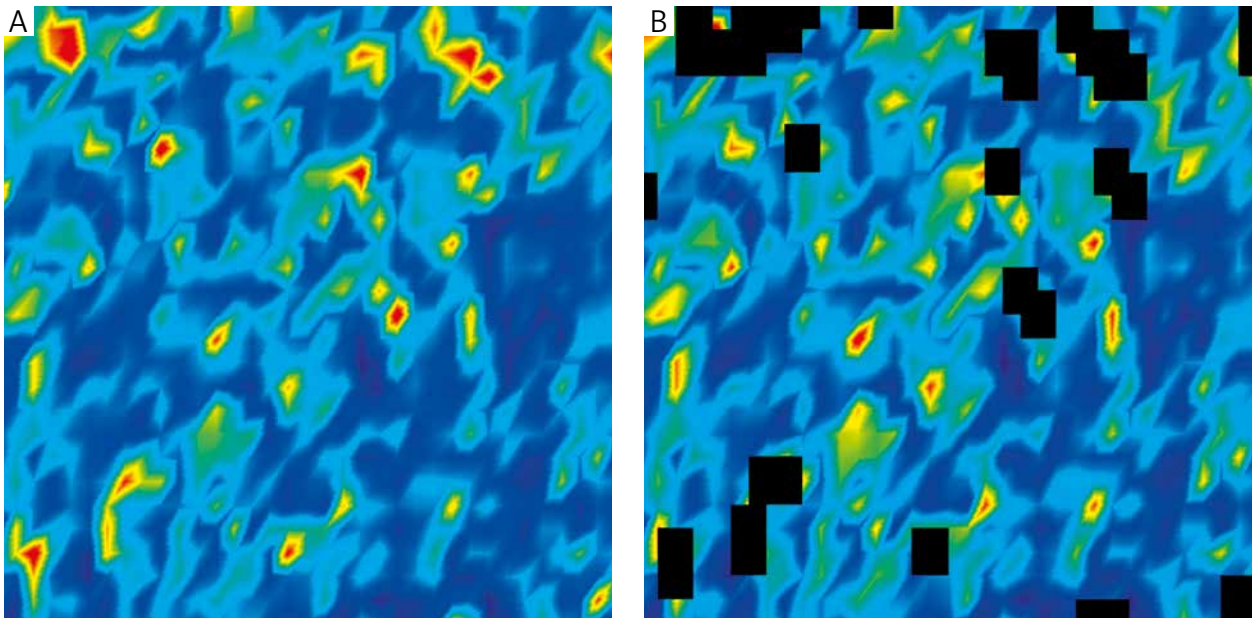

Fig. 1. Graphical presentation of results of the use of the sample thickness criterion: A) the chemical image of pheochromocytoma sample, B) the chemical image of pheochromocytoma sample with marked areas of sample not fulfilling the thickness criterion (black pixels)

Automatic baseline correction and automatic smoothing were used for preprocessing of the spectra, which were consequently used for further semi-quantitative analysis.

Statistical analysis

The statistical significance of the differences between medians of the analyzed parameters for all studied lesions was tested with the non-parametric Mann-Whitney U test at a significance level of 0.05. Non-parametric tests are used for variables which do not fulfill the normal distribution, as in the present analysis. According to the null hypothesis there is no statistically significant difference between groups. It is rejected when $p < 0.05$.

To determine which biochemical parameters contribute the most to the discrimination between the analyzed lesions, multiple discriminant analysis was applied. Prior to this kind of statistical analysis, the calculated values of parameters were transformed to log base 10. The logarithmic transformation was applied to make the distribution more symmetric and Gaussian-like, which was not fulfilled for raw data. Additionally, this procedure was applied to make the variances of the variables in the analyzed groups more homogeneous. The minimization of Wilks' λ was applied as the main criterion for determining the biochemical parameters contributing significantly to the discrimination between the analyzed groups of tissues. The forward stepwise procedure was used to determine discriminant functions for distinguishing between the analyzed groups of lesions.

Results

The differences in IR absorption spectra collected for the analyzed cases are shown in Figure 3. The averaged spectra from 20 representative points for each studied lesion are presented. The most pronounced differences are observed for two spectral ranges, i.e. between 2997 cm^{-1} and 2800 cm^{-1}, which corresponds to the lipid bands, as well as between 1770 cm^{1} and 1485 cm^{-1}, which are assigned mainly to the amide bands but also the lipid and nucleic acid bands. The level of lipids is higher in the adenoma and hyperplasia samples compared with pheochromocytoma cases (c.f. Fig. 3). In contrast, the pheochromocytoma samples are rich in proteins. As far as the range of lipids is quite easy to investigate, the region of amides is rather difficult to analyze due to the phenomenon of band overlapping. The absorption bands from the range between 1700 cm^{-1} and 1600 cm^{-1} originate from functional groups of various biological macromolecules.

Due to possible thickness distortion of the samples, the analysis was based only on the ratios of intensities of IR absorption bands or the ratios of the areas of absorption bands. The parameters used in the analysis are listed below:

- the ratio of 2997-2800 cm^{-1} to 1770-1485 cm^{-1} – lipids to proteins ratio as an indicator of the main differences between the cortical and medullar tissue type;
- the ratio of 1700-1600 cm^{-1} to 1580-1510 cm^{-1} – amide I to amide II ratio;
- the ratio of intensities of absorption bands at 2921 cm^{-1} to 2958 cm^{-1} – $\nu_{as}(CH_2):\nu_{as}(CH_3)$;
- the ratio of intensities of absorption bands at 3016 cm^{-1} to 2958 cm^{-1} – $\nu(=CH):\nu_{as}(CH_3)$;
- the ratio of intensities of absorption bands at 1654 cm^{-1} to 1631 cm^{-1} – α to β secondary structure of proteins;
- the ratio of intensities of absorption bands at 1045 cm^{-1} to 1081 cm^{-1} – glycogen/phosphate ratio;
- the ratio of intensities of absorption bands at 1121 cm^{-1} to 1020 cm^{-1} – RNA to DNA content.

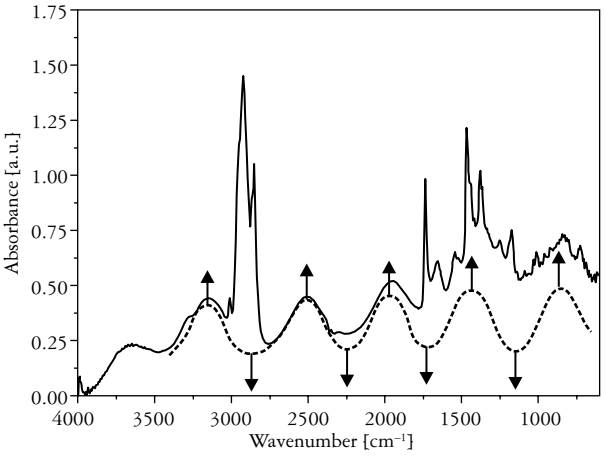

Fig. 2. Exemplary IR absorption spectrum of adenoma sample with visible scattering manifestation ("sinusoidal" baseline)

The preprocessed (as described above in paragraph 2.2) absorption spectra were analyzed to obtain the above-mentioned parameters. Then for every studied lesion the median values of those parameters were determined. In Fig. 4 the results obtained for pheochromocytoma, adenoma and hyperplasia are presented (the median value, the first and third quartile, and the minimum and maximum value of analyzed parameters).

The results shown in Fig. 4A confirm the higher content of lipids in adenoma and hyperplasia cases compared to the pheochromocytomas. A similar relation was found for the ratio of the absorption bands of amide I and amide II (c.f. Fig. 4B).

As far as the lipid related bands are concerned, it seems that the ratio of $\nu(=CH):\nu_{as}(CH_3)$ (3016 cm^{-1}/ 2958 cm^{-1}) is the highest for pheochromocytoma and decreases in adenoma and hyperplasia cases (see Fig.

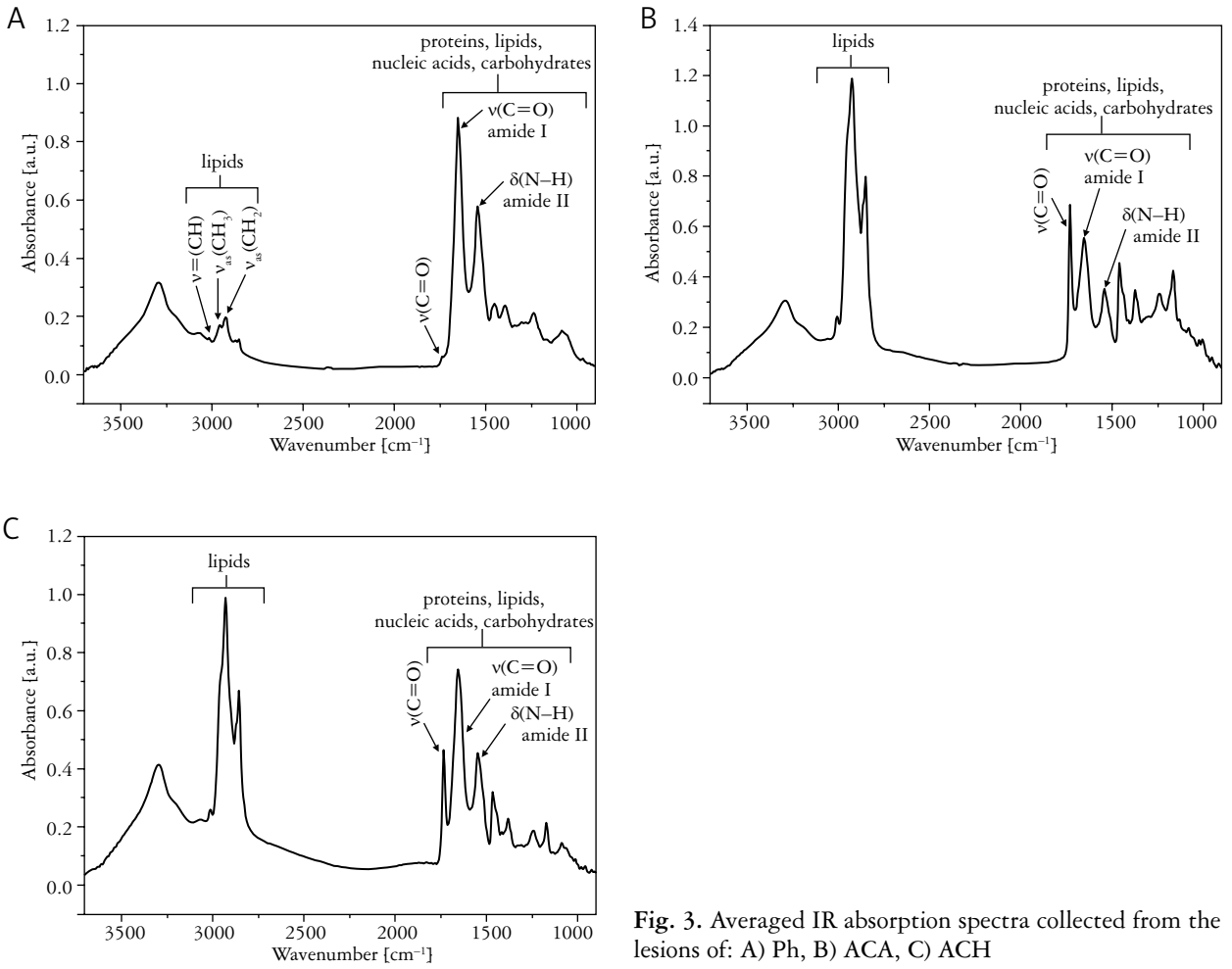

Fig. 3. Averaged IR absorption spectra collected from the lesions of: A) Ph, B) ACA, C) ACH

4C). Conversely, the ratio of $\nu_{as}(CH_2):\nu_{as}(CH_3)$ (2921 cm^{-1}/2958 cm^{-1}) for hyperplasia seems to be at the highest level, which decreases slightly in pheochromocytoma and adenoma (c.f. Fig. 4D).

The ratio of intensities of α to β secondary structure of proteins (1654 cm^{-1}/1631 cm^{-1}) is slightly higher for the adenoma samples compared to the pheochromocytoma and hyperplasia cases (Fig. 4E). From Fig. 4F it seems that the RNA/DNA (1121 cm^{-1}/1020 cm^{-1}) ratio is almost at the same level in all studied lesions. The glycogen/phosphate ratio in Fig. 4G (1045 cm^{-1}/1081 cm^{-1}) is lower in cortical derived tissue and higher in medullar pheochromocytoma.

On the basis of statistical analysis described earlier, it is possible to determine the statistically significant differences between the investigated groups (c.f. Table II).

The next statistical tool applied was multiple discriminant analysis. All biochemical parameters excluding the RNA/DNA ratio were included in the model built, and all of them were statistically significant in the discrimination. The values of partial Wilks' λ, the F-test of partial Wilks' λ and its p-values are summarized in Table III. It was found that the lipid/protein ratio is the most significant parameter in the general discrimination of lesion type. The ratios CH/CH3, α/β and CH2/CH3 were next in order of importance.

Two discriminant functions that express a linear combination of the values of biochemical parameters included in the model built were determined. The equations of the discriminant functions are as follows:

$$L_1 = 1.17*[\text{lipids/proteins}] - 0.47*[\nu(=CH):\nu_{as}(CH_3)] - 0.32*[\alpha/\beta \text{ proteins' secondary structure}] + 0.097*[\nu_{as}(CH_2):\nu_{as}(CH_3)] - 0.32*[\text{amide I/amide II}] - 0.28*[\text{glycogen/phosphate}]$$

$$L_2 = -0.045*[\text{lipids/proteins}] + 0.085*[\nu(=CH):\nu_{as}(CH_3)] + 0.71*[\alpha/\beta \text{ proteins' secondary structure}] - 0.72*[\nu_{as}(CH_2):\nu_{as}(CH_3)] + 0.43*[\text{amide I/amide II}] + 0.29*[\text{glycogen/phosphate}]$$

As can be seen, lipids/proteins and CH/CH_3 are the most significant biochemical parameters in the first discrimination function, whereas in the second one they are α/β and CH_2/CH_3 ratios.

A simple scatter plot between two discrimination variables was used for the examination of the group

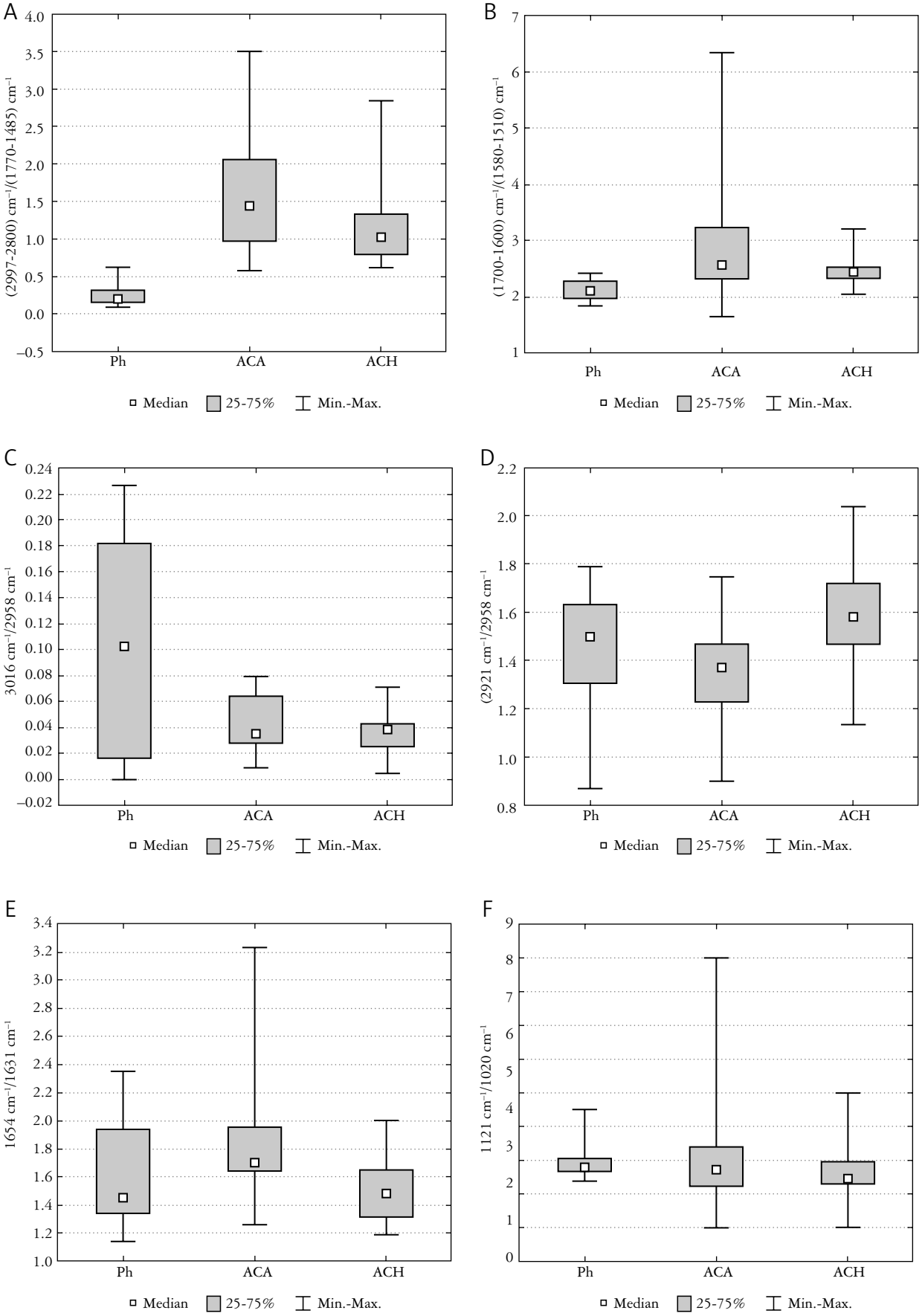

Fig. 4. The median values of ratios of IR absorption bands for pheochromocytoma (Ph), adenoma (ACA), hyperplasia (ACH)
{continued on the next page}

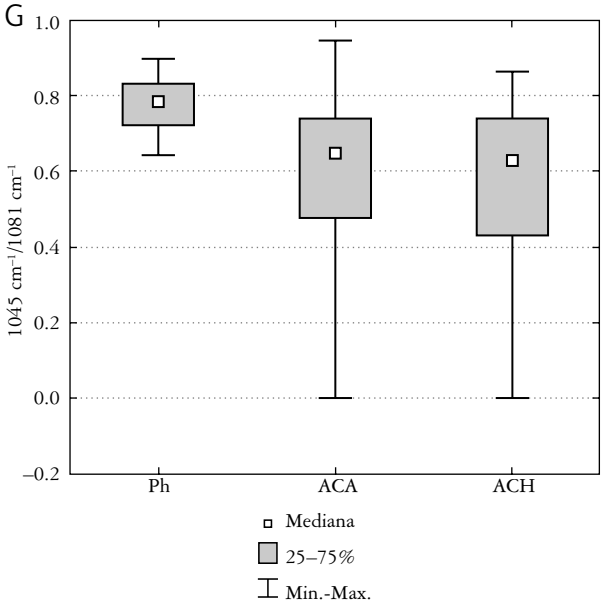

Fig. 4. *{continued}* The median values of ratios of IR absorption bands for pheochromocytoma (Ph), adenoma (ACA), hyperplasia (ACH)

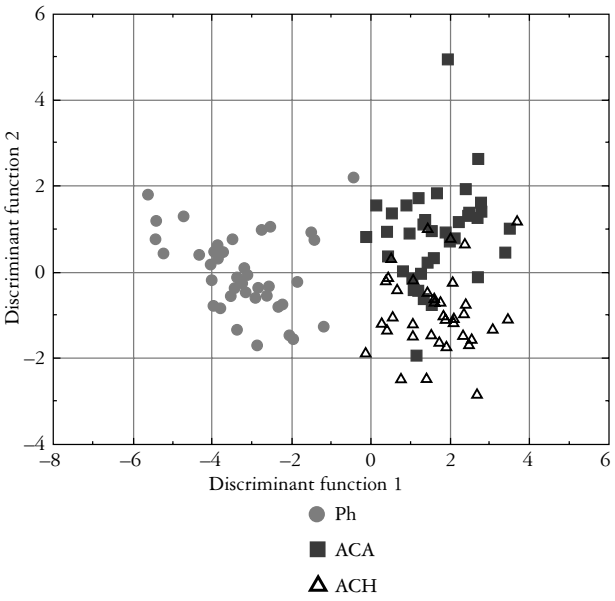

Fig. 5. Graphical presentation of two discrimination variables used for the examination of the group discrimination

discrimination. The results are illustrated in Fig. 5. The scatter plot shows that discriminant function 1 discriminates most between pheochromocytoma and the two other analyzed lesions (the greatest distance in the horizontal direction). The calculated values of means for discriminant function 1 were – 3.2 for Ph, 1.65 for ACA and 1.63 for ACH. In the vertical direction (discriminant function 2) points representing Ph, ACA and ACH lesions are located at a comparable level. Precisely, the calculated means for discriminant function 2 were as follows: 0.003 for Ph, 0.83 for ACA and –0.91 for ACH.

Discussion

According to the literature the potential biomarkers of pathological processes taking part in cancerogenesis can be attributed, among other things, to metabolic parameters, the level of lipid peroxidation and conformational changes in secondary protein structure [5].

The formation of a neoplasm is often connected with increased metabolism of the tissue. It is a consequence of rapid proliferation. Simultaneously, rapidly proliferating tissue requires an increased supply of oxygen. Different processes promote angiogenesis through the production of various vascular endothelial growth factors and specific receptors for them. When the tumor growth exceeds the formation of new microcirculation, hypoxia occurs. The state of hypoxia can imply many different molecular processes. Information about the metabolic parameters (for example glycogen, glucose, amino acids) as well as the products of cellular metabolism (lactic acids) can be obtained from the variation within the 1300-900 cm^{-1} FTIR spectral interval region.

Due to the higher glucose demand associated with rapid proliferation, the level of glycogen (1045 cm^{-1})

Table II. Results of Mann-Whitney U-test for comparisons of the analyzed groups of lesions

Parameter	Ph ↔ ACA	Ph ↔ ACH	ACA ↔ ACH
(2997-2800) cm^{-1}/(1770-1485) cm^{-1}	< 0.05	< 0.05	< 0.05
(1700-1600) cm^{-1}/(1580-1510) cm^{-1}	< 0.05	< 0.05	**0.07***
3016 cm^{1}/2958 cm^{-1}	< 0.05	< 0.05	**0.07***
2921 cm^{-1}/2958 cm^{-1}	< 0.05	< 0.05	< 0.05
(1654 cm^{-1}/1631 cm^{-1})	< 0.05	**0.30***	< 0.05
(1121 cm^{-1}/1020 cm^{-1})	**0.45***	< 0.05	**0.32***
(1045 cm^{-1}/1081 cm^{-1})	< 0.05	< 0.05	**0.85***

** the bold typed values mean a lack of statistically significant differences between studied lesions taking into consideration the analyzed parameter*

Table III. Results of multiple discriminant analysis

	Partial Wilks' lambda	F	p
(2997-2800) cm^{-1}/(1770-1485) cm^{-1}	0.266	148.62	<< 0.05
3016 cm1/2958 cm^{-1}	0.825	11.46	0.000031
1654 cm^{-1}/1631 cm^{-1}	0.783	14.91	0.000002
2921 cm^{-1}/2958 cm^{-1}	0.827	11.26	0.000036
(1700-1600) cm^{-1}/(1580-1510) cm^{-1}	0.903	5.83	0.0039
(1045 cm^{-1}/1081 cm^{-1})	0.920	4.67	0.011

is reduced, while simultaneously the phosphate content (1081 cm^{-1}) increases [14], as it is the skeletal part of forming carbohydrates. Furthermore, the elevated ratio of 1121 cm^{-1} and 1020 cm^{-1}, which reflects the RNA/DNA ratio, is believed to be a marker of neoplastic processes [5, 7]. In this paper both parameters were studied. The RNA/DNA ratio in all studied lesions was comparable, and this parameter was excluded from the discriminant functions. The ratio of absorption at around 1045 cm^{-1}/1081 cm^{-1} is lower for adenoma and hyperplasia cases, which can be attributed to the faster metabolic processes in cortical derived tumor cells. On the other hand, it seems that the metabolic rate for the pheochromocytoma cases is slower. It could mean that the neoplastic processes in the adrenal gland proceed at different rates according to the tumor type and especially the part of the adrenal gland from which the neoplastic lesion originates.

It is believed that oxidative stress precedes the neoplastic processes due to the reactive oxygen species (ROS) attack on cells. According to Petibois [15, 16], during oxidative stress a decrease in the CH_2/CH_3 ratio is observed, and it correlates with the increase in the CH/CH_3 ratio. What is more, the ratio of CH/CH_3 reflects the level of unsaturated lipids [5, 15], while the ratio of CH_2/CH_3 gives information on the lipid chain length [17]. The differences between the ratios of mentioned absorption bands, observed in the present study, could reflect some structural changes in lipids. The differences in CH_2/CH_3 ratio for three lesion types are not very clear. Nevertheless, the CH/CH_3 ratio is definitely the highest for the pheochromocytoma samples compared to the adenoma and hyperplasia samples, for which this ratio is at a comparable level.

The region of the amide I band (1600 – 1700 cm^{-1}) provides information on the secondary protein structure. Some authors report that the conformational changes of secondary protein structure could reflect the pathological states. For example, in Alzheimer disease the formation of β-amyloid is observed [18, 19]. In the present study the level of alpha to β proteins' secondary structure is higher for adenoma compared to the pheochromocytoma and hyperplasia cases. However, this relation is not simple. Remembering that adenoma tissue is rich in lipids, it is undisputable that lipids overlap the protein range of absorption bands (α and β secondary structures); hence it is not possible to make any far-reaching conclusions about the secondary structure of proteins in the studied samples. The way of overcoming this limitation is the special data treatment methods based on the curve-fitting procedures for determining the characteristic absorption of particular molecules [5]. Nevertheless, in the analysis presented in this paper there was no fitting procedure applied.

Our work is a pilot study and it gives only a general view of possible biomolecular differences between three types of adrenal gland lesions. On the basis of the performed study it was possible to find some specific biomolecular markers of different pathological processes in the adrenal gland. At the initial stage of research, it was only possible to find the differences between the studied tumor types, as hitherto there were no control samples available. In order to understand the pathological processes it is necessary to compare the results obtained for normal and pathological tissue. For more accurate and credible results it is advisable to increase the number of studied samples. Further research is in progress and will be published in a forthcoming article.

Conclusions

The measurements showed that the FTIR microspectroscopy is very fruitful for the study of biomolecular composition of adrenal gland lesions.

The results indicated the general differences between investigated tumor types within the range of lipid and protein absorption bands.

There is a tendency to a higher level of the ratio of α/β secondary protein structure in adenoma samples compared to pheochromocytoma and hyperplasia.

The decreased glycogen/phosphate ratio, assumed as an indicator of more intense cellular metabolic turnover, was observed for adenoma and hyperplasia samples, while for pheochromocytoma it was increased.

The differences in the ratio of CH/CH_3 and CH_2/CH_3 might suggest the conformational changes of lipids in all studied lesions.

There were almost no differences in the RNA/DNA ratio between the three lesion types.

For more reliable results the study should be continued and the number of studied samples should be increased.

Due to the high lipid content in adenoma and hyperplasia cases there was strong absorption observed within the lipid region ($\sim$2997-2800 cm^{-1}). Due to the complex architecture of tissue samples, diffraction artifacts were observed. To decrease the mentioned problem it is advisable to lower the sample thickness. There is an idea of preparing 6 μm thick tissue samples (the same thickness as used for standard histopathological examination).

There is a strong need to include a control group in the future research.

The authors declare no conflicts of interest.

This work was supported by the Polish Ministry of Science and Higher Education and its grants for Scientific Research.

References

1. Lack EE. Tumors of the Adrenal Glands and Extraadrenal Paraganglia, AFIP Atlas of Tumor Pathology, series 4. ARP Press Silver Spring, Maryland 2007; 1-35, 57-124, 241-274.
2. Fukumura D, Duda DG, Munn LL, et al. Tumor microvasculature and microenvironment: novel insights through intravital imaging in preclinical models. Microvasculation 2010; 17: 206-225.
3. Carmeliet P, Jain RK. Angiogenesis in cancer and other diseases. Nature 2004; 407: 249-257.
4. Sharma S, Sharma M, Sarkar C. Morphology of angiogenesis in human cancer: a conceptual overview, histoprognostic perspective and significance of neoangiogenesis. Histopathology 2005; 46: 481-489.
5. Petibois C, Déléris G. Chemical mapping of tumor progression by FT-IR imaging: towards molecular histopathology. Trends Biotechnol 2006; 24: 455-462.
6. Walsh M, German M, Singh M, et al. IR microspectroscopy: potential applications in cervical cancer screening. Cancer Lett 2007; 246: 1-11.
7. Walsh M, Singh M, Pollock H, et al. ATR microspectroscopy with multivariate analysis segregates grades of exfoliative cervical cytology. Biochem Biophys Res Commun 2007; 352: 213-219.
8. Das K, Kendall C, Martin I, et al. FTIR of touch imprint cytology: A novel tissue diagnostic technique. J Photoch Photobiol B Biol 2008; 92: 160-164.
9. Fabian H, Lasch P, Boese M, et al. Infrared microspectroscopic imaging of benign breast tumor tissue sections. J Mol Struct 2003; 661-662: 411-417.
10. Mackanos MA, Contag CH. FTIR microspectroscopy for improved prostate cancer diagnosis. Trends Biotechnol 2009; 27: 661-663.
11. Stuart B. Modern Infrared Spectroscopy. John Wiley & Sons, Chichester 1996.
12. Chwiej J, Dulinska J, Janeczko K, et al. Synchrotron FTIR micro-spectroscopy study of the rat hippocampal formation after pilocarpine-evoked seizures. J Chem Neuroanat 2010; 40: 140-147.
13. Lasch P, Haensch W, Nauman D, et al. Imaging of colorectal adenocarcinoma using FTIR microspectroscopy and cluster analysis. Biochim Biophys Acta 2004; 1688: 176-186.
14. Yano K, Ohoshima S, Shimizu Y, et al. Evaluation of glycogen level in human lung carcinoma tissues by an infrared spectroscopic method. Cancer Lett 1996; 110: 29-34.
15. Petibois C, Déléris G. Evidence that erythrocytes are highly susceptible to exercise oxidative stress: FT-IR spectrometric studies at the molecular level. Cell Biol Int 2005; 29: 709-716.
16. Petibois C, Déléris G. Erythrocyte adaptation to oxidative stress in endurance training. Arch Med Res 2005; 36: 524-531.
17. Kneipp J, Lasch P, Baldauf E, et al. Detection of pathological molecular alterations in scrapie-infected hamster brain by Fourier transform infrared (FT-IR) spectroscopy. Biochim Biophys Acta 2000; 1501: 189-199.
18. Choo LP, Wetzel DL, Halliday WC, et al. In situ characterization of beta-amyloid in Alzheimer's diseased tissue by synchrotron Fourier transform infrared microspectroscopy. Biophys J 1996; 71: 1672-1679.
19. Miller LM, Wang Q, Telivala TP, et al. Synchrotron-based infrared and X-ray imaging shows focalized accumulation of Cu and Zn co-localized with β-amyloid deposits in Alzheimer's disease. J Struct Biol 2006; 115: 30-37.

Address for correspondence

Magdalena B. Białas
Chair of Pathomorphology
Jagiellonian University, Medical College
Grzegórzecka 16
31-531 Krakow, Poland
e-mail: mbialas7@gmail.com